IOP Publishing Nanotechnology
Nanotechnology 27 (2016) 505705 (8pp) doi:10.1088/0957-4484/27/50/505705

Temperature measurement of Joule heated silicon micro/nanowires using selectively decorated quantum dots

Jeonghoon Yun[1,2], Jae-Hyuk Ahn[3], Bong Jae Lee[1], Dong-Il Moon[4], Yang-Kyu Choi[4] and Inkyu Park[1,2]

[1] Department of Mechanical Engineering, Korea Advanced Institute of Science and Technology (KAIST), Daejeon 305-701, Korea
[2] KAIST Institute for the Nanocentury (KINC), Korea Advanced Institute of Science and Technology (KAIST), Daejeon 305-701, Korea
[3] Department of Electronic Engineering, Kwangwoon University, Seoul 01897, Korea
[4] Department of Electrical Engineering, Korea Advanced Institute of Science and Technology (KAIST), Daejeon 305-701, Korea

E-mail: inkyu@kaist.ac.kr

Received 23 July 2016, revised 17 October 2016
Accepted for publication 1 November 2016
Published 21 November 2016

Abstract

We developed a novel method to measure local temperature at micro/nano-scale regions using selective deposition of quantum dots (QDs) as a sensitive temperature probe and measured the temperature of Joule heated silicon microwires (SiMWs) and silicon nanowires (SiNWs) by this method. The QDs are selectively coated only on the surface of the SiMWs and SiNWs by a sequential process composed of selective opening of a polymethyl methacrylate layer via Joule heating, covalent bonding of QDs, and lift-off process. The temperatures of the Joule-heated SiMWs and SiNWs can be measured by characterizing the temperature-dependent shift of photoluminescence peak of the selectively deposited QDs even with far-field optics. The validity of the extracted temperature has been also confirmed by comparing with numerical simulation results. The proposed method can potentially provide micro/nanoscale measurement of localized temperatures for a wide range of electrical and optical devices.

S Online supplementary data available from stacks.iop.org/NANO/27/505705/mmedia

Keywords: temperature measurement, quantum dots, Joule heating, silicon nanowires, microheater, nanoheater

(Some figures may appear in colour only in the online journal)

Introduction

Microheater devices have been widely used in thermal stimulation devices [1], microfluidic devices for the polymerase chain reaction [2] and miniaturized sensors such as gas sensors [3], humidity sensors [4] and flow sensors [5, 6] because of their fast heating/cooling speeds, localized heating confinement and low power consumption. Furthermore, nanoscale heaters such as Joule heated nanowires also have been used to fabricate highly integrated nanostructure arrays [7] and to detect gas molecules with enhanced performances [8, 9]. Accordingly, accurate temperature measurement of micro/nano-scale heating devices is very important, and thus a number of methods with micro/nano-scale resolutions have been developed for this purpose. Examples include high resolution infrared camera imaging [10], thermal reflectance measurement [11], temperature dependent liquid crystal imaging [12], scanning thermal microscopy [13] and spectral measurement of temperature dependent quantum dots (QDs) [14–16]. Infrared camera measures the peak wavelength or intensity of thermal radiation spectrum and converts them to a temperature. The temperature measurement techniques by

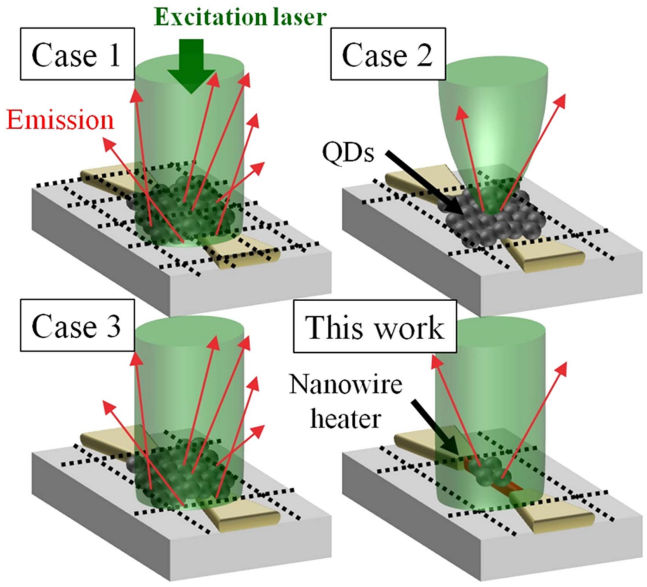

Figure 1. Representation of proposed method compared with three different types of conventional equipment setups for temperature measurement: (Case 1) high spatial resolution detector (grid indicates resolution of detector) with large excitation beam; (Case 2) low spatial resolution detector with ultrafine excitation beam; (Case 3) low spatial resolution detector with large excitation beam. In this work, neither ultrafine excitation beam nor high spatial resolution detector is required because QDs are coated only on the heated micro/nano-scale area.

thermal reflectance, liquid crystal imaging and spectral analysis of QDs utilize the temperature dependent reflectance of surface, crystallinity of polymer and band gap energy of QDs, respectively. The spatial resolutions of all of these optical temperature measurement methods are limited by the diffraction limit of emission spectrum, and a precise detector or highly focused excitation beam are required for measuring micro/nano-scale heated area. Thus, near-field measurement method such as scanning thermal microscopy has been utilized to measure nanoscale heated area by attaching temperature-sensing elements at the scanning probe tip [13, 17]. Although the scanning thermal microscopy has a high spatial resolution, its measurement accuracy is limited due to the heat dissipation via scanning probe tip and real-time measurement is difficult due to a long scanning time.

As mentioned above, QDs have been utilized as a non-contact temperature probe since their bandgap energy is dependent on the temperature [18–20]. When the QDs are deposited on a device and irradiated by laser, the temperature of the device can be extracted by measuring the photoluminescence spectra of the QDs [14–16]. Figure 1 shows the schematic of our method in comparison to other conventional methods based on the spectral shift of QDs. In order to measure the micro/nano-scale heated area using this method, the emission spectra of QDs from micro/nano-scale heated areas and non-heated areas should be distinguished. Thus, the spatial resolution of optical detector should be micro/nano-scale (case 1 in figure 1) or the laser beam should be focused only on the desired micro/nano-scale hot spots (case 2 in figure 1). Otherwise, the emission spectra of QDs from non-heated area become stronger than that from the micro/nano-scale heated area (case 3 in figure 1). However, the optical detectors with high spatial resolutions are highly complicated and expensive, and the excitation beam with sub-wavelength focal spot size also requires specialized equipment and stringent experimental control. Although a near-field measurement technique can measure the temperature of nanoscale heated area, the measurement procedure is much more complicated than the far-field measurement. In order to resolve this limitation, we have proposed a novel method by selectively depositing QDs on desired micro/nano-scale hot spots ('this work' in figure 1). By using our method, neither a highly focused excitation beam nor a probe with high spatial resolution is required. Specifically, QDs are selectively deposited on the Joule heated area of a silicon microwire (SiMW) or silicon nanowire (SiNW) through thermal decomposition of polymer passivation layer and chemical bonding of QDs on the surface, followed by lift-off process. We measure the Joule heating dependent photoluminescence of QDs on the Joule heated SiMW/SiNWs and calculate their temperatures by using the temperature dependent bandgap energy of QDs. The temperature dependence of photoluminescence peak of QDs is characterized and the temperature function of bandgap is calculated, from which the temperature of SiMWs/SiNWs is estimated.

Experimental

We fabricated SiMW/SiNWs by top-down micro/nano-fabrication processes. SiMWs were fabricated by using silicon on insulator (SOI, top silicon device layer = 50 nm and buried oxide layer = 400 nm) substrate. The patterns of SiMWs were defined by photolithography and reactive ion etching. Fabricated SiMWs had an average width of 4.2 μm, length of 5 μm, thickness of 45 nm and were doped with p-type dopants (ion implantation, boron, $\rho = 7 \times 10^{-2}\,\Omega \cdot \mathrm{cm}$). Source and drain regions were highly doped with p-type dopants (ion implantation, boron, $\rho = 6 \times 10^{-4}\,\Omega \cdot \mathrm{cm}$) for ohmic contact with metal electrodes and decrease of resistance except for the microwire region. Rapid thermal annealing (1000 °C, 10 s in N_2 environment) was used for the dopant activation. Thermal oxidation and forming gas annealing were utilized to grow 9 nm thick silicon oxide layer on the SiMW with reduction of top silicon layer and to passivate dangling bonds generated at the boundary between silicon and silicon oxide layer. Gold electrodes for electrical probing were patterned by using photolithography, vacuum deposition of chromium (10 nm) and gold (200 nm) by electron beam evaporation, and lift-off process. The SiNWs were also fabricated by similar CMOS compatible fabrication processes using SOI (top silicon layer = 40 nm and buried oxide layer = 140 nm) wafer, except for the nanolithography process instead of photolithography. Specifically, SiNWs were fabricated by deep ultraviolet lithography, time-controlled photoresist ashing, and reactive-ion etching [9]. Fabricated SiNWs had an average width of 120 nm, length of 2 μm and thickness of 40 nm, and were doped with n-type dopants (ion implantation,

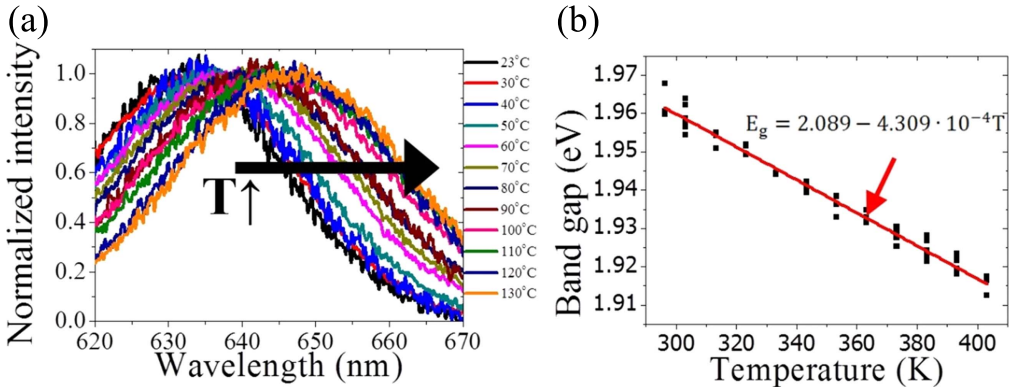

Figure 2. Temperature dependence of QD photoluminescence: (a) normalized photoluminescence results of QDs on a bare silicon wafer by increasing the temperature from 23 °C to 130 °C and (b) band gap energy ($E = hc/\lambda = (1239.8\,\text{eV nm})/\lambda$) of QDs having a linear relationship with the temperature (E(eV) = 2.089–4.309 × 10^{-4} T(K)).

phosphorus, $\rho = 1 \times 10^{-2}\,\Omega \cdot \text{cm}$). Source and drain regions were highly doped with n-type dopants (ion implantation, arsenic, $\rho = 6 \times 10^{-4}\,\Omega \cdot \text{cm}$) for ohmic contact with probing tips and decrease of resistance except for the nanowire region. Rapid thermal annealing (1000 °C, 10 s in N_2 environment) was used for the dopant activation. Thermal oxidation and forming gas annealing were utilized to grow 3 nm thick silicon oxide layer on the SiNW and to passivate dangling bonds, respectively.

Polymethyl methacrylate (PMMA, MicroChem) used as a passivation polymer layer was coated on the SiMW and SiNW devices by spin coating with a thickness of 140 nm. PMMA layer was selectively decomposed only along the Joule-heated SiMW/SiNWs [21]. For the surface modification of exposed silicon oxide layer with amine group, the devices was immersed in an ethanol diluted solution of 3-aminopropyl triethoxysilane (Sigma Aldrich) for 2 h and rinsed with ethanol and deionized water several times. QDs (Emfutur) composed of cadmium selenide (CdSe; core) and zinc sulfide (ZnS; shell) with an average diameter of 6.0 nm were utilized. For chemical bonding with amine-modified silicon surface, the surface of ZnS layer of QDs was modified with a carboxyl group by thioctic acid (Sigma-Aldrich) [22]. Carboxyl-modified QDs were immobilized on the amine-modified silicon substrate with a crosslinking agent of 1-ethyl-3-(3-dimethylaminopropyl) carbodiimide (EDC) [23]. Finally, PMMA layer was removed by dipping the device into acetone while the QDs were remained on the SiMW/SiNWs via covalent bonding. Figure S1 in the online supplementary data shows the schematic of QDs coating processes.

In order to characterize the temperature dependent photoluminescence of QDs, they were coated on a bare silicon wafer. Then, the silicon wafer was mounted on a small heater and while the substrate temperature was measured by using a k-type thermocouple attached on the substrate. We can assume that the temperature of QDs is the same as that of the top surface of silicon wafer due to very small thickness (~20 nm) of QD film. Afterwards, the photoluminescence of QDs was characterized with a 514 nm laser as an excitation light source while increasing the temperature. For characterizing the photoluminescence of QDs on the Joule heated SiMWs/SiNWs, electrical bias was applied on the QD coated SiMWs/SiNWs by using a source meter (Keithley 2400) while the photoluminescence of QDs was characterized with 514 nm laser as the excitation light source.

Results and discussion

Figure 2(a) shows the photoluminescence plots of the QDs on the heated silicon wafer. The emission wavelength of QDs is shifted to higher wavelength as the temperature is increased [19, 20]. The bandgap energy is decreased due to the dilatation of lattice structure as the temperature is increased [24]. The emission wavelength of QDs changes from 632 to 647 nm as the temperature is increased from 23 °C to 130 °C. The bandgap energy of QDs can be calculated by the Plank–Einstein relation ($E = hc/\lambda = (1239.8\,\text{eV nm})/\lambda$) and plotted as shown in figure 2(b). The bandgap energy of QDs shows a linear relationship with temperature and is fitted as the function of temperature in the following:

$$E\,(\text{eV}) = 2.089\text{–}4.309 \times 10^{-4}\,T\,(\text{K}). \quad (1)$$

This empirical function is used for the temperature estimation of Joule heated SiMW/SiNW devices.

As explained above, QDs were selectively coated on the SiMW/SiNWs by self-assembly and lift-off of QDs. PMMA was used as a lift-off layer and selectively removed by thermal decomposition through Joule heating of SiMW/SiNWs as shown in figures 3(a) and (b). The Joule heating of SiMW/SiNWs generates localized heating along the wires and the local temperature is raised sufficiently for the thermal decomposition of PMMA. Here, the PMMA layer was decomposed by applying a DC bias of 43 V (0.985 mA) for the SiMW and by a DC bias of 11.5 V (0.177 mA) for the SiNW. Figures 3(a-(i), (ii)) and (b-(i), (ii)) show the optical microscope images of SiMW/SiNWs before and after selective opening of PMMA layer by their Joule heating. The AFM images clearly indicate local thermal decomposition of PMMA along Joule heated SiMW/SiNWs (online supplementary figure S2). A possible residual layer on the SiMW/SiNW surface after decomposition of PMMA was completely

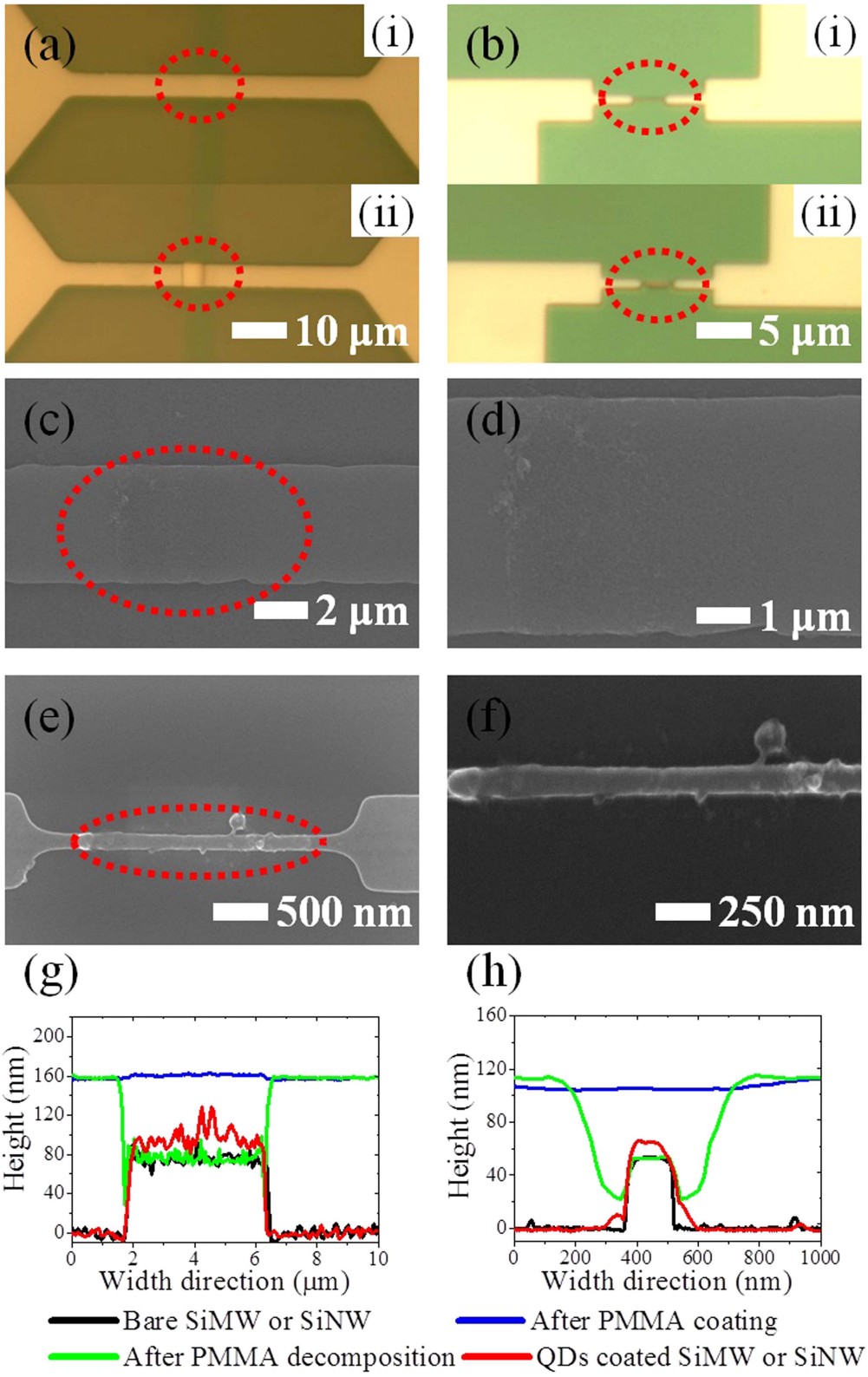

Figure 3. Selective coating of QDs on the SiMW and SiNW by thermal decomposition of PMMA layer via Joule heating of SiMW/SiNW: (a), (b) Microscope images of PMMA decomposition by Joule heating of SiMW and SiNW: (i) before decomposition and (ii) after decomposition. (c)–(f) SEM images of QDs selectively coated on the SiMW and SiNW (red dotted contour indicates QDs coated region). (g), (h) Line profiles of SiMW (g) and SiNW (h) after each step of sequential QD coating process. PMMA layer is decomposed only along the Joule heated SiMW and SiNW, and QDs are coated only on the SiMW and SiNW after the lift-off process.

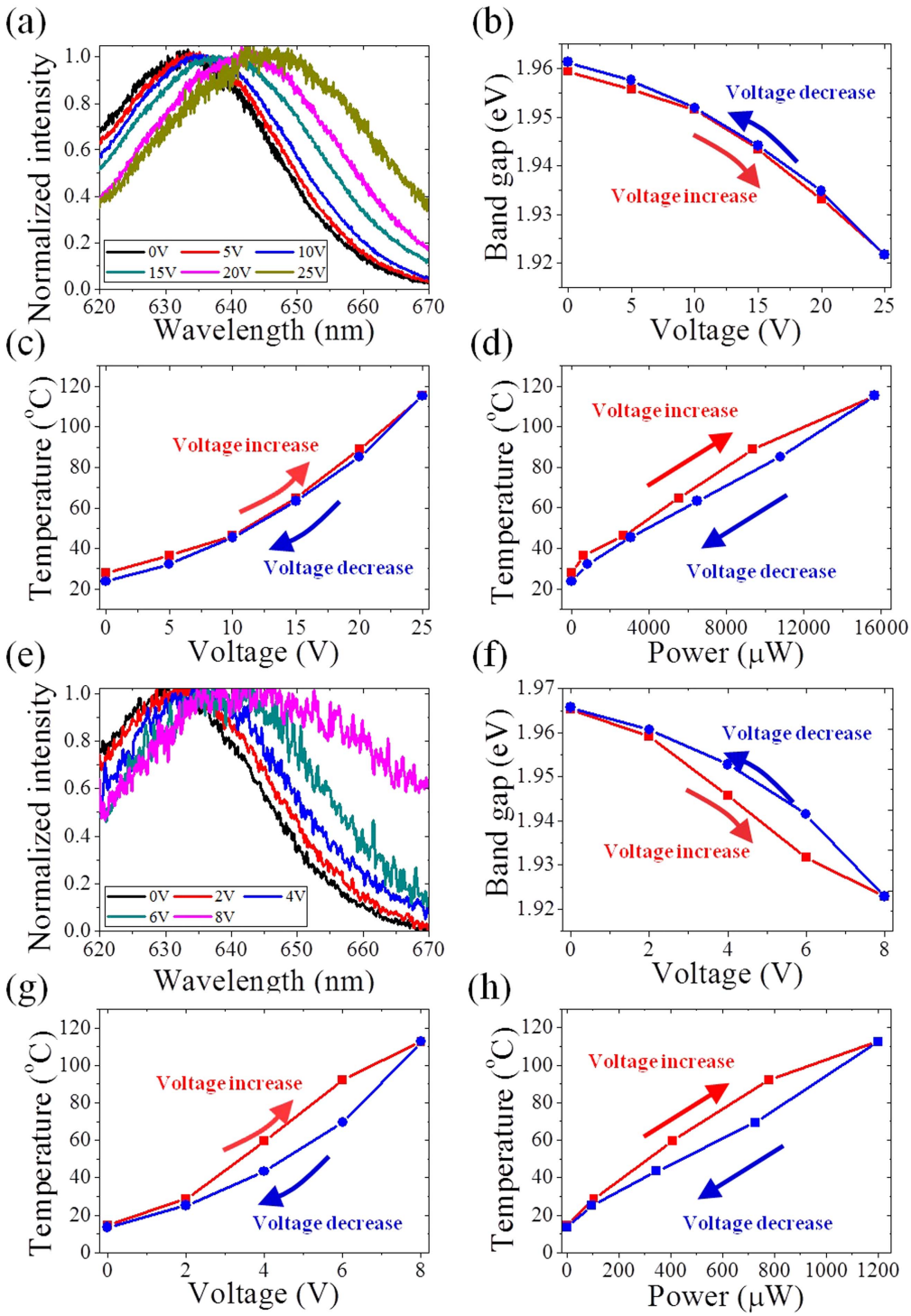

Figure 4. Temperature measurement of SiMW/SiNW by QD photoluminescence measurement: (a) normalized photoluminescence of Joule heated SiMW; (b) Joule heating dependent bandgap energy of QDs on SiMW; (c) Joule heating voltage versus temperature of SiMW; (d) Joule heating power versus temperature of SiMW; (e) normalized photoluminescence of Joule heated SiNW; (f) Joule heating dependent bandgap energy of QDs; (g) Joule heating voltage versus temperature of SiNW; (h) Joule heating power versus temperature of SiNW. Here, the arrows represent the voltage sweeping directions.

removed from the SiMW/SiNW surface by a short-term oxygen plasma etching process (10 W, 30 s). We confirmed the selective coating of QDs by the SEM images (figures 3(c)–(f)). Figures 3(g) and (h) show the cross-sectional line profiles of bare SiMW/SiNW, those after PMMA coating, those after thermal decomposition of PMMA layer, and those after QD coating from AFM imaging. The line profiles of the QD coated SiMW/SiNW prove that the QDs are coated only on the SiMW/SiNW. Also, the differences of the line profiles before and after QD coating show that the heights of QD layer on SiMW/SiNW are approximately

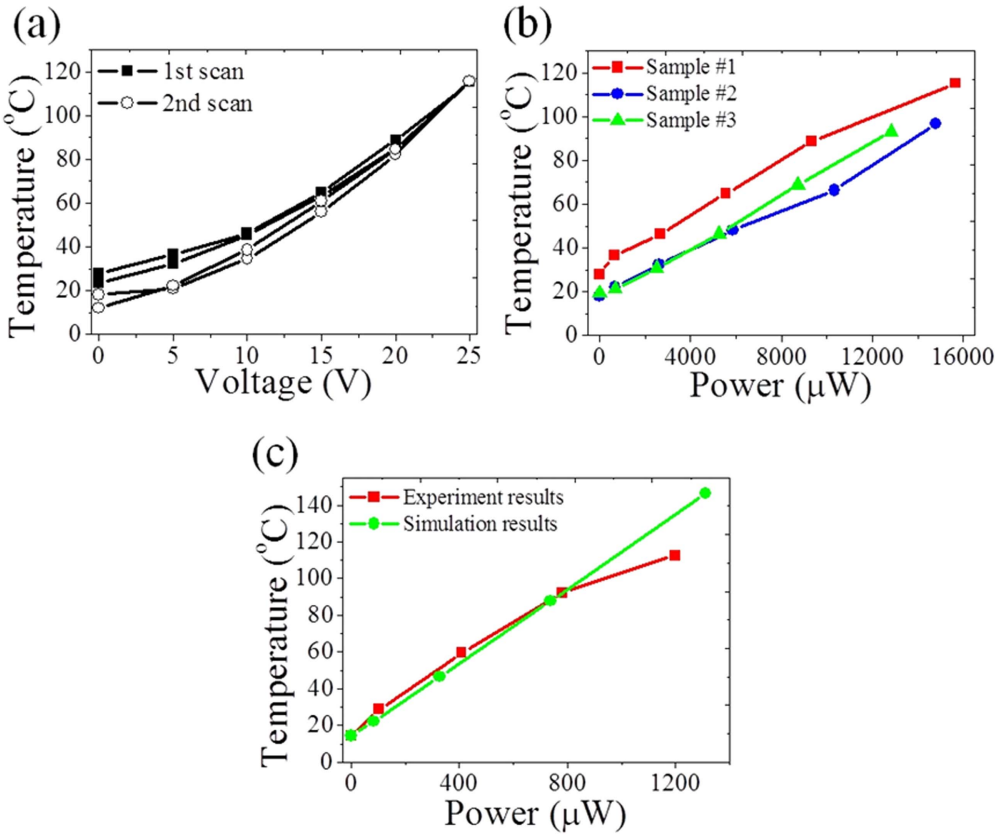

Figure 5. Reliability of temperature measurement by using this method: (a) repetitive temperature measurement of the same SiMW through two cycles of experiments, (b) repeatability confirmed by repeating the temperature measurement for three different SiMWs, (c) computer simulation of Joule heated SiNW with selectively coated QDs on the SiNW compared with the experiment results.

20 nm and 10 nm, respectively (online supplementary figure S3).

After the selective coating of QDs on the Joule-heated SiMW/SiNWs, their photoluminescence is characterized as shown in figure 4. Figure 4(a) shows the normalized photoluminescence (I/I_{peak}) of the QDs while increasing the applied voltage across the SiMW from 0 to 25 V (0.59 mA). The bandgap shift of QDs is observed to be from 1.959 to 1.922 eV due to the Joule heating of SiMW as shown in figure 4(b). The temperature of QDs is calculated by the empirical function (equation 1) of temperature. Figure panels 4(c) and (d) show the temperature–voltage and temperature–power relations in the SiMW, respectively. The temperature of SiMW should be a linear function of applied power because most of the Joule heating energy is dissipated via thermal conduction and convection in microscale, and this is experimentally verified as shown in figure 4(d). The measured temperature of SiMW is well fitted as a linear function of the Joule heating power. However, it should be also noted that the temperature of SiMW may not be exactly a linear function of Joule heating power because the resistivity of the SiMW is increased by the phonon scattering due to Joule heating at high voltage conditions. Red and blue curves in figures 4(b)–(d) represent the temperature of SiMW measured by increasing and decreasing the Joule heating voltage, respectively, and this reveals a small hysteresis of the temperature measurement, presumably due to the photo-oxidation of QDs.

The temperature of SiNW is also measured by the same method as shown in figures 4(e)–(h). Figure 4(e) shows the change of normalized photoluminescence (I/I_{peak}) of SiNW when the applied voltage is increased from 0 to 8 V (0.147 mA). In contrast, no emission wavelength shift by Joule heating of the SiNW is observed in the photoluminescence measurement from QDs that are nonselectively coated on the SiNW (i.e. QDs are coated on the SiNW as well as in the surrounding of SiNW) (online supplementary figure S4). A bandgap shift of QDs from 1.965 to 1.923 eV occurs due to the Joule heating of SiNW as shown in figure 4(f). We can find a linear relationship between the temperature and power applied to the SiNW as shown in figure 4(g). Even though the power supplied to the SiNW is much smaller than that supplied to the SiMW, the temperature of SiNW can reach similar value as that of the SiMW due to much smaller heat capacity of the SiNW. In addition, we observe larger hysteresis of temperature while the applied power is increased and then decreased (red and blue curves). This may be due to smaller amount of QDs on SiNW than on SiMW, which may have caused higher measurement error.

We confirmed the repeatability of this method for the temperature measurement of Joule-heated SiMWs. Figure 5(a) shows the result of repeated temperature measurement of a SiMW by two scanning cycles. The first and second temperature measurement cycles of a SiMW show similar Joule heating voltage–temperature dependency, but

the temperature at the second measurement cycle is lower than that from the first measurement cycle. It has been found that the QDs tend to gradually degrade under laser irradiation or high temperature conditions [25–28]. An oxidation of QDs under laser irradiation in ambient condition and a blue shift of emission wavelength by the oxidation were reported in the previous study [27]. Shorter wavelength corresponds to lower temperature in the empirical function (1) and thus the temperature is underestimated in the second scanning cycle than the first cycle. We can conclude that the temperature measurement using QDs is useful for the short-term temperature characterization rather than repetitive or long-term temperature measurement. We have confirmed the reliability of our temperature measurement method by repetitive temperature measurement of three different SiMWs as shown in figure 5(b). Temperature measurement results of the three SiMWs are not exactly the same due to the geometrical difference of microfabricated devices. However, the slopes of linear fitting for temperature versus power are almost identical with 4% of difference. Figure 5(c) displays the numerical calculation of Joule heated SiNW in comparison with the measured temperature for different electrical power (detail of numerical simulation is explained in the supporting information (online supplementary figures S5–S7)). Here, it should be noted that the plotted simulation result is the average temperature along the channel region of Joule-heated SiNW and the experimental result is the average temperature of QDs that are coated on thermally decomposed region. Although there is some discrepancy at high heating power ($>1200\ \mu$W), the experimental and simulation results generally show good agreement with each other, verifying the validity of measured temperature by using our method.

In summary, we developed a novel method to measure the temperature of Joule heated SiMW/SiNWs by selective coating of QDs on the heated area of SiMW/SiNWs. Selective coating of QDs can be achieved simply by the thermal decomposition of polymer layer via Joule heating of the SiMW/SiNWs, followed by the deposition and lift-off of QDs. This temperature measurement does not require complicated laser focusing or precise stage control because QDs are selectively coated only on the heated micro/nano-scale areas. We have confirmed the repeatability and reliability of this measurement method and good agreement with the numerical calculation based on finite element method. It is expected that this simple approach would have a great potential for probing localized temperature of various micro/nano-electronic devices such as microheaters for integrated gas sensors, self-heated nanomaterial-based chemical sensors, phase-change memory devices, etc.

Acknowledgments

This research was supported by Nano Material Technology Development Program (2015M3A7B7045518) and Center for Optically-assisted Ultrahigh-precision Mechanical Systems (2015R1A5A1037668) through the National Research Foundation of Korea (NRF) funded by the Ministry of Science, ICT & Future Planning, and a part of the project titled 'Development of Management Technology for HNS Accident' funded by the Ministry of Oceans and Fisheries, Korea.

References

[1] Ginet P, Montagne K, Akiyama S, Rajabpour A, Taniguchi A, Fujii T, Sakai Y, Kim B, Fourmy D and Volz S 2011 Towards single cell heat shock response by accurate control on thermal confinement with an on-chip microwire electrode *Lab Chip* **11** 1513–20

[2] Bu M, Montagne K, Akiyama S, Rajabpour A, Taniguchi A, Fujii T, Sakai Y, Kim B, Fourmy D and Volz S 2011 Design and theroretical evaluation of a novel microfluidic device to be used for PCR *J. Micromech. Microeng.* **13** S125–30

[3] Lim M A, Kim D H, Park C O, Lee Y W, Han S W, Li Z, Williams R S and Park I 2012 A new route toward ultrasensitive, flexible chemical sensors: metal nanotubes by wet-chemical synthesis along sacrificial nanowire templates *ACS Nano* **6** 598–608

[4] Dai C-L, Liu M-C, Chen F-S, Wu C-C and Chang M-W 2007 A nanowire WO_3 humidity sensor integrated with micro-heater and inverting amplifier circuit on chip manufactured using CMOS-MEMS technique *Sensors Actuators* B **123** 896–901

[5] Mailly F, Giani A, Bonnot R, Temple-Boyer P, Pascal-Delannoy F, Foucaran A and Boyer A 2001 Anemometer with hot platinum thin film *Sensor Actuators* A **94** 32–8

[6] Kim T H and Kim S J 2006 Development of a micro-thermal flow sensor with thin-film thermocouples *J. Micromech. Microeng.* **16** 2502–8

[7] Jin C Y, Yun J, Kim J, Yang D, Kim D H, Ahn J H, Lee K C and Park I 2014 Highly integrated synthesis of heterogeneous nanostructures on nanowire heater array *Nanoscale* **6** 14428–32

[8] Yun J, Jin C Y, Ahn J H, Jeon S and Park I 2013 A self-heated silicon nanowire array: selective surface modification with catalytic nanoparticles by nanoscale Joule heating and its gas sensing applications *Nanoscale* **5** 6851–6

[9] Ahn J H, Yun J, Moon D I, Choi Y K and Park I 2015 Self-heated silicon nanowires for high performance hydrogen gas detection *Nanotechnology* **26** 095501

[10] FLIR Systems www.flir.com

[11] Park H, Lee B J and Lee J 2014 Note: simultaneous determination of local temperature and thickness of heated cantilevers using two-wavelength thermoreflectance *Rev. Sci. Instrum.* **85** 036109

[12] Elibol O H, Reddy B and Bashir R 2008 Localized heating and thermal characterization of high electrical resistivity silicon-on-insulator sensors using nematic liquid crystals *Appl. Phys. Lett.* **93** 131908

[13] Majumdar A 1999 Scanning thermal microscopy *Annu. Rev. Mater. Sci.* **29** 505–85

[14] Saidi E, Babinet N, Lalouat L, Lesueur J, Aigouy L, Volz S, Labeguerie-Egea J and Mortier M 2011 Tuning temperature and size of hot spots and hot-spot arrays *Small* **7** 259–64

[15] Li S, Zhang K, Yang J M, Lin L W and Yang H 2007 Single quantum dots as local temperature markers *Nano Lett.* **7** 3102–5

[16] Woo J Y, Tripathy S K, Kim K and Han C-S 2012 Thermal and structural dependence of the band gap of quantum dots measured by a transparent film heater *Appl. Phys. Lett.* **100** 063105

[17] Yoon K, Hwang G, Chung J, Kim H G, Kwon O, Kihm K D and Lee J S 2014 Measuring the thermal conductivity of residue-free suspended graphene bridge using null point scanning thermal microscopy *Carbon* **76** 77–83

[18] Walker G W, Sundar V C, Rudzinski C M, Wun A W, Bawendi M G and Nocera D G 2003 Quantum-dot optical temperature probes *Appl. Phys. Lett.* **83** 3555

[19] Valerini D, Cretí A, Lomascolo M, Manna L, Cingolani R and Anni M 2005 Temperature dependence of the photoluminescence properties of colloidal CdSe/ZnScore/shell quantum dots embedded in a polystyrene matrix *Phys. Rev.* B **71** 235409

[20] Narayanaswamy A, Feiner L F and van der Zaag P J 2008 Temperature dependence of the photoluminescence of InP/ZnS quantum dots *J. Phys. Chem.* C **112** 6775–80

[21] Jin C Y, Li Z, Williams R S, Lee K C and Park I 2011 Localized temperature and chemical reaction control in nanoscale space by nanowire array *Nano Lett.* **11** 4818–25

[22] Mattoussi H, Mauro J M, Goldman E R, Anderson G P, Sundar V C, Mikulec F V and Bawendi M G 2000 Self-assembly of CdSe-ZnS quantum dot bioconjugates using an engineered recombinant protein *J. Am. Chem. Soc.* **122** 12142–50

[23] Panchaud A, Hansson J, Affolter M, Bel Rhlid R, Piu S, Moreillon P and Kussmann M 2008 ANIBAL, stable isotope-based quantitative proteomics by aniline and benzoic acid labeling of amino and carboxylic groups *Mol. Cell. Proteomics* **7** 800–12

[24] Varshni Y P 1967 Temperature dependence of the energy gap in semiconductors *Physica* **34** 149–54

[25] Zhao Y, Riemersma C, Pietra F, Koole R, Donega Cde M and Meijerink A 2012 High-temperature luminescence quenching of colloidal quantum dots *ACS Nano* **6** 9058–67

[26] Kohary K and Gibson G A 2011 Modelling photooxidation of CdSe-ZnS nanocrystals *Phys. Status Solidi* C **8** 2569–71

[27] van Sark W G J H M, Frederix P L T M, Van den Heuvel D J, Gerritsen H C, Bol A A, van Lingen J N J, Donega C D and Meijerink A 2001 Photooxidation and photobleaching of single CdSe/ZnS quantum dots probed by room-temperature time-resolved spectroscopy *J. Phys. Chem.* B **105** 8281–4

[28] Nazzal A Y, Wang X Y, Qu L H, Yu W, Wang Y J, Peng X G and Xiao M 2004 Environmental effects on photoluminescence of highly luminescent CdSe and CdSe/ZnS core/shell nanocrystals in polymer thin films *J. Phys. Chem.* B **108** 5507–15